Chaos, Solitons and Fractals 103 (2017) 622–631

Contents lists available at ScienceDirect

Chaos, Solitons and Fractals

Nonlinear Science, and Nonequilibrium and Complex Phenomena

journal homepage: www.elsevier.com/locate/chaos

Multi-fractal geometry of finite networks of spins: Nonequilibrium dynamics beyond thermalization and many-body-localization

Paul Bogdan[a,*], Edmond Jonckheere[a], Sophie Schirmer[b]

[a] Ming Hsieh Department of Electrical Engineering, University of Southern California, Los Angeles, CA 90089, USA
[b] College of Science (Physics), Swansea University, Singleton Park, Swansea SA2 8PP, UK

ARTICLE INFO

Article history:
Received 17 September 2016
Revised 15 June 2017
Accepted 7 July 2017

Keywords:
Quantum spin networks
Information capacity
Fractals
Phase transitions
Nanodevices
Nano-networks
Beyond Turing computation

ABSTRACT

Quantum spin networks overcome the challenges of traditional charge-based electronics by encoding information into spin degrees of freedom. Although beneficial for transmitting information with minimal losses when compared to their charge-based counterparts, the mathematical formalization of the information propagation in a spin(tronic) network is challenging due to its complicated scaling properties. In this paper, we propose a fractal geometric approach for unraveling the information-theoretic phenomena of spin chains and rings by abstracting them as weighted graphs, where the vertices correspond to single spin excitation states and the edges represent the information theoretic distance between pair of nodes. The weighted graph exhibits a complex self-similar structure. To quantify this complex behavior, we develop a new box-counting-inspired algorithm which assesses the mono-fractal versus multi-fractal properties of quantum spin networks. Mono- and multi-fractal properties are in the same spirit as, but different from, Eigenstate Thermalization Hypothesis (ETH) and Many-Body Localization (MBL), respectively. To demonstrate criticality in finite size systems, we define a thermodynamics inspired framework for describing information propagation and show evidence that some spin chains and rings exhibit an informational phase transition phenomenon, akin to the MBL transition.

1. Introduction

1.1. Motivation–spintronics networks

Many fundamental particles such as electrons, protons and certain atomic nuclei exhibit a fundamental quantum property called spin. Spin degrees of freedom have played an important role since the discovery of nuclear magnetic resonance [19] and electron spin resonance [3], which have become essential tools for characterizing chemical structure, material properties and bio-medical imaging [10,20,22]. More recently, spin degrees of freedom have been in the spotlight again as potential carriers of quantum information, and the foundation of quantum spintronics [2].

Conventional electronics, while powerful, also has drawbacks. Electrical resistance encountered by moving electrons generates heat, wasting energy and limiting integration densities and data processing speeds in conventional semiconductor devices [25]. Spintronics in its most basic form is about exploiting spin degrees of freedom, usually of electrons, to encode, process, store and transfer information. Encoding information in spin degrees of freedom such as excitations of a spin network opens up many possibilities [15,17], where spintronics devices offer benefits such as generally long coherence lifetimes of spins at low temperatures. Although there are many technological challenges that remain to be solved, considerable efforts are currently under way to realize various types of spintronic devices [2].

The spintronic property that propagation happens without matter or charge transport makes spintronic networks potentially attractive for more efficient on-chip interconnectivity via “spin channels” even for classical information processing. In this context one of the most important questions is the capacity of a spin(tronic) network for information transport or teleportation of quantum states between nodes in the network. The transport can happen under intrinsic dynamics, but in order to make the transport more efficient, couplings in spin chains can be “engineered” to achieve, at the limit, perfect state transfer between end points [8,9,16]. For example, a chain with nearest-neighbor couplings satisfying [9]

$$J_{k,k+1} = \frac{1}{2}\sqrt{k(N-k)}, \quad k = 1, \ldots, N-1, \tag{1}$$

achieves this objective [9]. Rings can be biased to “quench” the ring to a chain to favor transfer to a particular spin [15,18].

* Corresponding author.
E-mail address: pbogdan@usc.edu (P. Bogdan).

http://dx.doi.org/10.1016/j.chaos.2017.07.008

One measure introduced to capture the intrinsic ability of a quantum network to transport information between nodes through the propagation of excitations is Information Transfer Fidelity (ITF) [11–13,15,18]. Broadly, it is an easily computable upper bound on the maximum achievable probability with which an excitation can be successfully propagated from one node to another in the network.

The ITF induces a (pra)metric [15, Section 4.1] for the spin network that endows it with an information topology. This information topology of the spin network generally differs substantially from the physical geometry of the network [11].

1.2. Mono and multi-fractals in spintronics networks

With very high order metric network graphs comes the question of scaling of their properties. For example, a network might be negatively curved in the very large scale sense of Gromov, but have different local curvature properties. Referring more specifically to spin networks, a device that has a cluster of excited spins might look like thermalized at a low scale, while the same cluster rather looks like localized at a larger scale. The present paper essentially addresses such questions. The essential tool is that of multi-fractal analysis. We show that the node-to-node interactions in such "symmetric" spin networks as long chains and rings exhibit self-similarity characterized by a narrow fractal spectrum, indicating mono-fractal behavior, consistent with ETH, Eigenstate Thermalization Hypothesis [27–29]. Shorter chains tend to have broader fractal spectra. However, the multi-fractal property takes its full significance when the chain or the ring is manipulated—in a way that affects symmetry or translation invariance—to favor specific transmissions, consistently with MBL, Multi-Body Localization [27].

While the phenomena that our fractal analysis exposes bear similarity with ETH and MBL, they are not *strictly speaking* ETH and MBL. The chief difference can be summarized as ETH and MBL being *equilibrium phenomena*, whereas the phenomena we here expose are *nonequilibrium phenomena*. This comparison is made precise in Section 3.5.

1.3. Paper outline

The paper is organized as follows. We begin, in Section 2, with the information geometry embedding of quantum spin networks. We provide the basics of the mathematical description of the Information Transfer Fidelity between quantum spin excitation states. Building on this background, in Section 3, we present the multi-fractal characteristics of this information geometry embedding and a greedy algorithm for investigating the multi-fractality of quantum spin networks, along with a novel box counting measure different from the popular one [24]. We also compare our nonequilibrium approach with such equilibrium procedures as Anderson localization and strong multi-fractal Multi-Body Localization. In the next two Sections 4 and 5, we detail our multi-fractal analysis of quantum chains and quantum rings, respectively, under various network sizes and various manipulations to favor some selective transfers. In Section 6, we attempt to define a transition from thermalization to localization [27–29]. We conclude the paper, in Section 7, by discussing the deeper significance of our results, outlining our main findings, and indicating several future research directions.

2. Information geometry embedding of spin networks

If we encode information in the states of a quantum system such as a network of N coupled spin-$\frac{1}{2}$ particles, then the transfer of information between quantum states is governed by the Schrödinger equation,

$$\imath\hbar\frac{d}{dt}|\psi(t)\rangle = H|\psi(t)\rangle, \quad |\Psi(0)\rangle = |i\rangle, \quad \imath = \sqrt{-1} \tag{2}$$

or a suitable open-system generalization [6]. In the preceding, $|i\rangle$ denotes the state where the only single excitation in the network is on spin i. The evolution from initial state $|i\rangle$ is characterized by a Hamiltonian H, a Hermitian operator with eigendecomposition

$$H = \sum_{n=1}^{\bar{N}} \lambda_n \Pi_n, \quad \bar{N} \leq N, \tag{3}$$

where the λ_n's are the (distinct) real eigenvalues and the Π_n's are the corresponding projectors onto the corresponding eigenspaces. The problem of capturing the t^* that yields maximum fidelity $\sup_{t\geq 0}|\langle j|\exp(-\imath Ht/\hbar)|i\rangle|$ in the temporal evolution of a given input state $|i\rangle$ is complicated; for this reason, we derive an easily computable upper bound on the probability of transfer of information, irrespective of the time it takes, to another state $|j\rangle$ in a network governed by the Hamiltonian H,

$$\sup_{t\geq 0}|\langle j|\exp(-\imath Ht/\hbar)|i\rangle|^2 \leq p_{\max}(i,j) := \sum_{k=1}^{\bar{N}}|\langle j|\Pi_k|i\rangle|^2. \tag{4}$$

Conditions for attainability of the bound in homogeneous chains and rings are derived in [11] and [15], respectively.

Taking the logarithm of the transition probability, we can define an Information Transfer Fidelity (ITF) "distance"

$$d(i,j) = -\log p_{\max}(i,j). \tag{5}$$

Note that $p_{\max}(i,i) = 1$ for any state $|i\rangle$ as $\sum_{k=1}^{\bar{N}}\Pi_k$ is a resolution of the identity, and also that $p_{\max}(i,j) = p_{\max}(j,i)$. Hence $d(i,i) = 0$ and $d(i,j) = d(j,i) \geq 0$, so that $d(\,\cdot\,,\,\cdot\,)$ is a symmetric prametric [1, p. 23]. Although this prametric need not be separating [1, p. 23], that is, $d(i,j) = 0$ need not imply $i = j$ as it happens for anti-podal points of N even spin rings, the latter is easily fixed by identifying those $d(i,j) = 0$ points. After this identification, the resulting semi-metric in general does not satisfy the triangle inequality, but for certain types of homogeneous networks it has been shown to induce a proper metric [12,15]. For the purposes of our analysis here a semi-metric (which by definition satisfies all axioms except the triangle inequality) is sufficient. To make the exposition more crisp, we will from here on, with a slight abuse of language, refer to $d(\,\cdot\,,\,\cdot\,)$ as determined by Eq. (5) as a distance.

In what follows, we set forth a fractal geometrical approach to the spin network in the sense that the information interactions within the spin network are represented as a weighted graph $\mathcal{G} = (\mathcal{V}, \mathcal{E})$, where the vertices represent spin excitation states and the edges denote their information-theoretic semi-metric.

Although our approach and the mathematical techniques employed are general and can be applied to any spin network, in this work we focus on simple networks such as linear arrangements (chains) or circular arrangements (rings) of spins with nearest-neighbor interactions, for which the J-coupling matrix is either tridiagonal (chain) or circulant (ring). For a network with uniform coupling all non-zero entries in the J matrix are the same, and we can choose units such that they are 1. More generally, we can always choose units such that the maximum coupling strength is 1. If the dynamics of the network are restricted to the single excitation subspace then the Hamiltonian on this subspace is determined by the J-coupling matrix; for Heisenberg coupling there are additional non-zero elements on the diagonal, while the diagonal elements are zero for XX-type coupling [5].

2.1. Extreme cases of thermalization and localization

The ITF between nodes i and j in a network can be physically interpreted as follows. If we create a local excitation at node i at

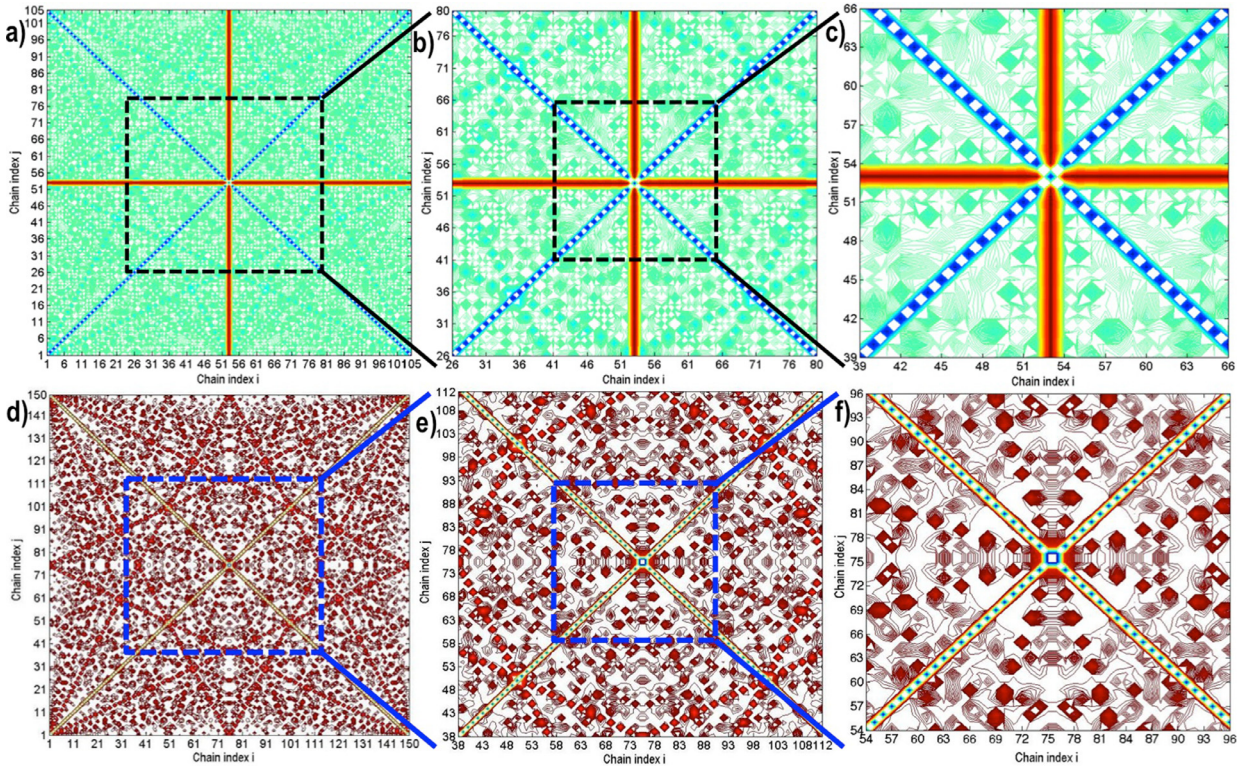

Fig. 1. (a) Realization of the ITF for a spin chain of size $N = 105$. (b) Zoom-in magnification on the ITF metric graph by a factor of 2. (c) Zoom-in magnification on the ITF metric graph by a factor of 4. (d) Realization of the ITF for a spin chain of size $N = 150$. (e) Zoom-in magnification of the ITF graph realization by a factor of 2. (f) Zoom-in magnification of the ITF graph realization by a factor of 4.

$t = 0$, by flipping the ith spin in the network, then the ITF $p_{\max}(i, j)$ is the maximum probability of excitation of spin j that can be observed as a result for any $t \geq 0$. In the special case when an excitation at node i remains localized at node i, we have $p_{\max}(i, j) = \delta_{ij}$. More generally, if an excitation remains confined to a subset nodes, e.g., in the case of Many Body Localization (MBL), then the maximum transition probability to all other nodes should be 0. In the opposite case of thermalization, the initial excitation will spread over the entire network and we expect $p_{\max}(i, j)$ to be the same for all $j \neq i$. However, there are many cases inbetween these two extremes, as will be shown in Section 6.

3. Fractal analysis

One important characteristic exhibited by the information distance graph representation of spin networks is the *self-similarity* of the node-to-node interactions. In mathematical context, the self-similarity implies that an object (process) is exactly or approximately similar to a subcomponent under the magnification operation (the whole resemblance in shape to subcomponents). Fig. 1 shows a visual representation of the information distance for spin chains of size $N = 105$ and $N = 150$, respectively. Although different network sizes exhibit different spatial interaction patterns, the metric graph representation is not entirely irregular under the magnification operation; rather it exhibits repetition and symmetry—there are information valleys surrounded by hill tops that seem to repeat almost identically across space, yet are not exactly identical. From a mathematical perspective, we know that this irregularity cannot be understood by simply defining the embedding dimension as the number of variables and coordinates as considered in [13], but rather calls for quantifying the dimension using multi-fractal geometry [21].

3.1. Information distance mapping

To investigate the multi-fractal characteristics of spin networks, we adopt the following strategy. As shown in Fig. 2, after the metric mapping, the information metric-based graph representation of the spin network can also be seen as a map of contour lines (isolines), where two nodes connected by an information distance (weight) less than or equal to $d(i, j)$ belong to an island (bounded by a closed contour line) encompassing all nodes within the same $d(i, j)$ distance. Second, we construct a graph-based box-covering renormalization inspired method [21,23], which aims at covering the metric graph with a minimum number of boxes $B_k(\epsilon)$ of radius [1] $\epsilon = d(i, j)$ for a predefined set of distances $d(i, j)$. This procedure records first the unique magnitudes of the exhibited weights (i.e., radii $d(i, j)$) in the graph and for each such magnitude finds the minimum number of boxes required to cover all nodes in the graph. To minimize the computational (search) time for the minimum number of boxes, we use a greedy heuristic, which for each magnitude of the box prunes the original weighted graph by removing the edges that exceed the magnitude and clusters the nodes that are connected by weighted edges smaller than the current magnitude. The algorithm then proceeds by analyzing and covering each cluster in descending order of their size (number of nodes). Knowing the number of boxes required to cover the weighted graph for each magnitude of the box allows us to investigate the multi-fractality and determine (estimate) the generating function of the counting measure as a function of the box radius.

[1] Throughout the explanation of the multi-fractal analysis, we use the concept of radius to denote all nodes which can be reached within one hop search because their distances (weights) to the center node under investigation is less than the specific radius.

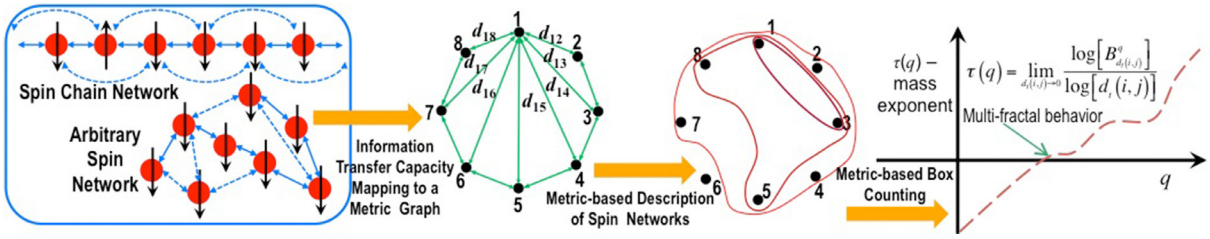

Fig. 2. An arbitrary spin network with a set of heterogeneous coupling parameters can be represented using information-theoretic measures as a weighted graph. Depending on the time dependent probability of transfer of excitation from spin $|i\rangle$ to $|j\rangle$ and the information theoretic measure defined on these node-to-node interactions, some nodes may reside in a smaller geodesic island even though spatially they reside at a much larger physical distance. Relying on the information theoretic measure, a box counting inspired strategy can help to investigate the scaling behavior of the mass exponent and derive the multi fractal spectrum associated with node-to-node interactions in a spin network.

Note that nodes that appear to be close to each other in the spin network domain representation may belong to different islands of concentration as a function of the adopted metric (e.g., information transfer distance). For instance, while nodes 1 and 2 are adjacent to each other in the original spin network (see Fig. 2), in the distance-based representation they may be further apart from each other. Although in Fig. 2 and throughout our current analysis we used only the information transfer metric defined above, the mathematical framework can be applied to other information-theoretic metrics and can be extended to analyze weighted graphs that can be generated by spin network interactions over time.

3.2. Node counting measure

The multi-fractal analysis rests on a novel *node (counting) measure* defined as follows:

$$\mu[B_k(\epsilon)] = \frac{N_k(\epsilon)}{N} = p_k(\epsilon), \tag{6}$$

where ϵ represents the magnitude of the information distance, $B_k(\epsilon) = \{\ell \in \mathcal{V} : d(k,\ell) \le \epsilon\}$ denotes a ball of radius ϵ centered in node $k \in \mathcal{V}$ and of ITF radius ϵ, N is the total number of nodes in the spin network or weighted graph $\mathcal{G}$, and $N_k(\epsilon)$ denotes the number of nodes inside the ball $B_k(\epsilon)$ of ITF radius ϵ. To put it in other words, $p_k(\epsilon)$ represents the probability of finding a node ℓ in the ball $B_k(\epsilon)$. Of note, this probability satisfies: $\sum_k [p_k(\epsilon)^q]_{q=1} = 1$ and $\sum_k [p_k(\epsilon)^q]_{q=0} = N$, respectively. This counting measure bears similarities with and extends the multi-fractal formalism presented in [7] such that the mass property is replaced by the counting of nodes covered by a ball of a certain radius on the graph. A similar strategy can be generalized to hypergraphs, but this is left for future work.

For a multi-fractal graph structure, the node counting measure satisfies the following relationship:

$$\mu[B_k(\epsilon)] = c_{k,\alpha_k}\epsilon^{\alpha_k}, \text{ as } \epsilon \to 0, \tag{7}$$

where α_k denotes the Lipschitz–Hölder exponent and c_{k,α_k} is a coefficient that depends on the box and the Lipschitz–Hölder exponent α_k. The Lipschitz–Hölder exponent can be defined for any measure μ and quantifies the singularity of the measure, here the singularity of the informational geometry.

The partition function can be expressed as:

$$Z(q,\epsilon) = \sum_k \{\mu[B_k(\epsilon)]\}^q = \sum_k \{c_{k,\alpha_k}\epsilon^{\alpha_k}\}^q, \tag{8}$$

where $q \in (-\infty, \infty)$ is a moment order and the summation is upper bounded by N representing the total number of boxes of size ϵ. Note that if $-\log \mu[B_k(\epsilon)]$ can be interpreted as an energy E_k, then $q \ge 0$ can be interpreted as an inverse thermal energy, $\beta = 1/k_B T$, where k_B is the Boltzmann constant and T the absolute temperature. The partition function then acquires a classical thermodynamical interpretation $\sum_k e^{-\beta E_k}$, from which phase transition can already be seen from the specific heat capacity curve of Fig. 5(b). Following this thermodynamic analogy, the free energy and the specific heat can be expressed as $F(q,\epsilon) = -\ln[Z(q,\epsilon)]/\ln[\epsilon]$ and $C(q,\epsilon) = -\partial^2 F(q,\epsilon)/\partial q^2$ [14], respectively.

By performing a histogram-like analysis (i.e., sorting and counting all terms corresponding to a particular Lipschitz–Hölder exponent α), the partition function takes the form:

$$Z(q,\epsilon) = \sum_\alpha \epsilon^{q\alpha} \sum_{k \in \mathcal{V}_\alpha} c_{k,\alpha}^q, \tag{9}$$

where $\mathcal{V}_\alpha$ represents the subset of vertices characterized by a Lipschitz–Hölder exponent α.

To manipulate the second sum, we define the multi-fractal spectrum $f(\alpha)$ to be the Hausdorff dimension of the set $\mathcal{V}_\alpha$. Recall that the Hausdorff dimension of a set $\mathcal{V}_\alpha$ is the unique dimension d_H such that the Hausdorff measure in dimension d at scale ϵ,

$$H_\epsilon^{d_H} = \inf_{\substack{\mathrm{diam}(B_k) < \epsilon \\ \cup_k B_k \supseteq \mathcal{V}_\alpha}} \sum_k (\mathrm{diam}(B_k))^{d_H},$$

is finite as $\epsilon \downarrow 0$. We attempt to write $H_\epsilon^{f(\alpha)} \sim \epsilon^{f(\alpha)} \times n_\alpha$, where n_α is the number of subsets in the covering. The finiteness of $H_\epsilon^{f(\alpha)}$ as $\epsilon \downarrow 0$ implies that $n_\alpha \sim \epsilon^{-f(\alpha)}$; more precisely,

$$n_\alpha = \text{number of balls of radius } \epsilon = w(\alpha)\epsilon^{-f(\alpha)},$$

with $f(\alpha)$ denoting the multi-fractal spectrum. It provides the distribution of the α's. Taking the spectrum $f(\alpha)$ to be narrowly distributed yields mono-fractality; taking it more spread yields multi-fractality.

Combining these derivations, the partition function becomes

$$Z(q,\epsilon) = \sum_\alpha b(q,\alpha) w(\alpha) \epsilon^{q\alpha - f(\alpha)}, \tag{10}$$

where $b(q,\alpha) = n_\alpha^{-1} \sum_{k \in \mathcal{V}_\alpha} c_{k,\alpha}^q$ is a coefficient that depends on the number of balls of size ϵ required for covering the graph embedding.

3.3. Mono-fractal versus multi-fractal distribution

The exponents of ϵ in Eq. (10) suggest to operate the Legendre transformation

$$\tau(q) = q\alpha - f(\alpha) \tag{11}$$

and look at the partition function in terms of the moment exponent q,

$$Z(q,\epsilon) = \sum_k \{\mu[B_k(\epsilon)]\}^q = g(q)\epsilon^{\tau(q)}, \tag{12}$$

where $\tau(q)$ is called the mass exponent function and is used to quantify the scaling properties of the partition function. As an alternative definition of mono versus multi-fractality, if the mass exponent $\tau(q)$ in Eq. (11) is a linear function of the q-exponent, then

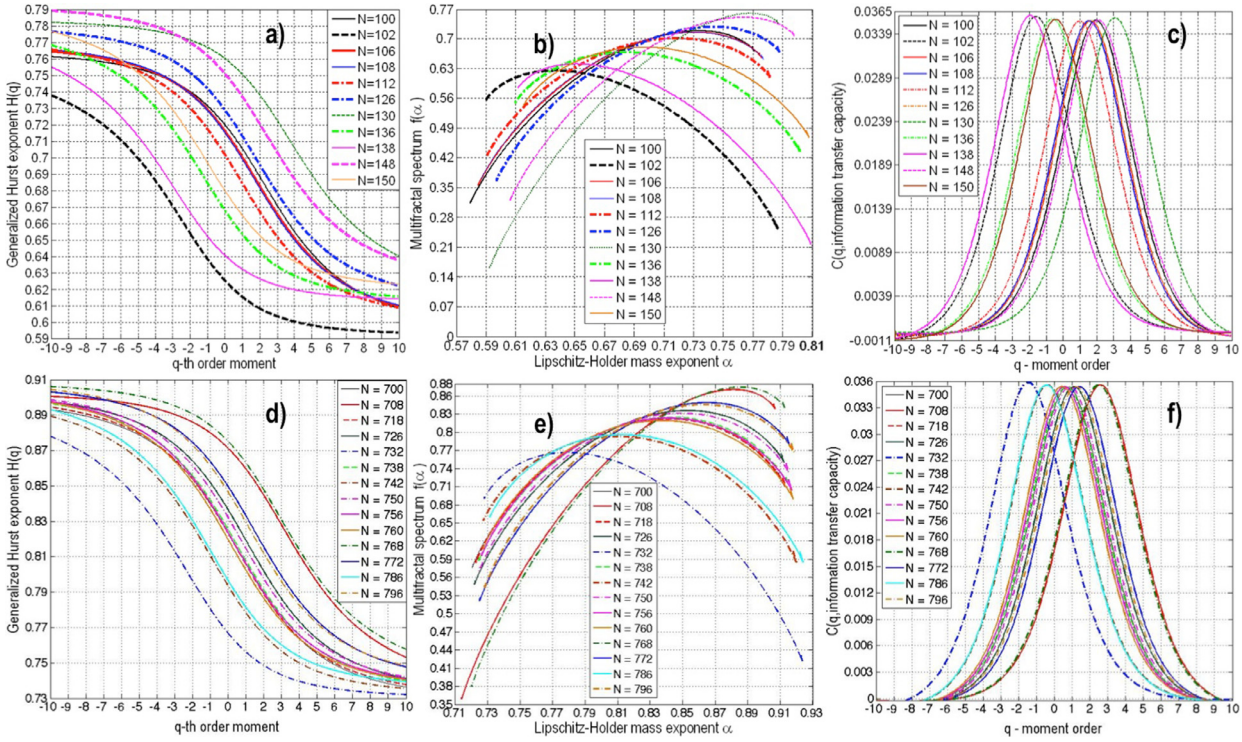

Fig. 3. (a) Generalized Hurst exponent $H(q)$ as a function of q for several spin chain lengths (i.e., $N = 100, 102, 106, 108, 112, 126, 130, 136, 138, 148, 150$) displaying a similar "sigmoidal" shape, but rich multi-fractal behavior. (b) Multi-fractal spectrum $f(\alpha)$ as a function of the Lipschitz-Hölder mass exponent α for several spin chain lengths (i.e., $N = 100, 102, 106, 108, 112, 126, 130, 136, 138, 148, 150$). Although spin chains exhibit similar multi-fractal spectrum, they are characterized by different dominant singularities (i.e., α at which $f(\alpha)$ attains maximum varies across spin chains). (c) Specific heat $C(q)$ for several lengths (i.e., $N = 100, 102, 106, 108, 112, 126, 130, 136, 138, 148, 150$) of a spin chain. (d) Generalized Hurst exponent $H(q)$ as a function of q for several spin chain lengths (i.e., $N = 700, 708, 718, 726, 732, 738, 742, 750, 756, 760, 768, 772, 786, 796$) displaying a similar "sigmoidal" shape, but rich multi-fractal behavior. (e) Multi-fractal spectrum $f(\alpha)$ as a function of the Lipschitz-Hölder mass exponent α for several spin chain lengths (i.e., $N = 700, 708, 718, 726, 732, 738, 742, 750, 756, 760, 768, 772, 786, 796$). (f) Specific heat $C(q)$ for several lengths (i.e., $N = 700, 708, 718, 726, 732, 738, 742, 750, 756, 760, 768, 772, 786, 796$) of the spin chain. Although the length of the spin chain varies significantly, we observe similar multi-fractal patterns and curvature in the specific heat.

we call the distribution of node measure $\mu[B_k(\epsilon)]$ to be mono-fractal. This typically happens when $f(\alpha)$ is δ-distributed. On the other hand, if the mass exponent $\tau(q)$ is a nonlinear function of the q-exponent, then we call the distribution of node measure $\mu[B_k(\epsilon)]$ to be multi-fractal.

3.4. Generalized Hurst exponent

The generalized Hurst exponent for time-series [4] is adapted to measures defined on graphs, with the objective of quantifying the roughness of the communication landscape. Following that thread, the generalized Hurst exponent $H(q)$ for the measure μ defined on the graph $\mathcal{G}$ is defined as

$$\left(\frac{1}{N}\sum_k \mu[B_k(\epsilon)]^q\right)^{1/q} = \epsilon^{H(q)}.$$

Technically, $H(q)$ provides the scaling of the q-order moments of the probability measure μ. The key insight coming from self-similarity of measure μ is to set $N\epsilon = \text{constant}$, say, 1. Then the above becomes

$$\sum_k \mu[B_k(\epsilon)]^q = \epsilon^{qH(q)-1}.$$

Comparing this with the definition of $\tau(q)$ provided by (12) yields

$$\tau(q) = qH(q) - 1. \tag{13}$$

The mass exponent function $\tau(q)$ is also related to the generalized dimension function $D(q)$ through the following equation: $\tau(q) = (q-1)D(q)$.

Based on the above-mentioned arguments, a linear dependence of the mass exponent $\tau(q)$ implies that the generalized Hurst exponent $H(q) = H$ is independent of the q-dependent exponents. In contrast, a nonlinear dependence of the mass exponent $\tau(q)$ implies that the generalized Hurst exponent will also exhibit a non-linearity with varying exponents q.

Investigation of the generalized Hurst exponent $H(q)$ is motivated by the need to quantify the spatial heterogeneity that may exist in an information metric based representation. Simply speaking, we aim to study how small and large fluctuations across all node interactions contribute to particular patterns that may appear over multiple scales and influence the dependence of $H(q)$ as a function of order q. Consequently, in our framework, the generalized Hurst exponent represents a mathematical approach for investigating the scaling properties and measuring the degree of heterogeneity of the graph motifs over multiple spatial scales. More precisely, if the analysis of the qth-order moments of the distribution of information graph motifs shows no dependence on the generalized Hurst exponent with the order of the moment q, then the informational graph is considered homogeneous and mono-fractal. In contrast, if the generalized Hurst exponent exhibits significant variation over a wide range of q orders, then the information graph is considered to be heterogeneous and multi-fractal. This multi-fractal structure (of the information based embedding of spin chains) can be understood as a divergence in terms of scaling trends between the short range (small fluctuations in ITF) and long-range (large fluctuations) ITF magnitudes.

3.5. Comparison with multi-fractal Anderson localization

Fluctuations around the metal-insulator criticality in Anderson localization is known to be multifractal [24]. While the fundamental mathematical techniques utilized in the latter are undoubtedly similar to ours, here, it is applied to a situation different from, although in the same spirit as, Anderson localization. First and most importantly, we do not deal with Anderson localization in the sense of fast spatial decay of eigenstate components $\psi_{\ell \neq k}$ away from site k; we rather deal with the number of sites ℓ within ITF $p_{\max} \approx 1-\epsilon$, away from k or within distance $d(k, \ell) \approx \epsilon$ from k.

To make the comparison crisp, consider the partition function shared by both approaches: $Z(q) = \sum_k \mu_k^q$, with $\mu_k = c_{k,\alpha_k} \epsilon^{\alpha_k}$. In [24, Section 3.1], the measure μ_k is $\sum_{\ell \in \mathrm{Box}_k(\epsilon)} |\psi_\ell|^2 \sim \epsilon^{\alpha_k}$ for ℓ in the box centered at site k of *physical* size ϵ, while here μ_k is the relative number $N_k(\epsilon)/N \sim \epsilon^{\alpha_k}$ of sites ℓ within the box of *ITF* size ϵ centered at k.

Clearly because of the discrepancy in the definition of the α_k's, the multifractal spectrum $f(\alpha)$ of localization cannot be expected to be the same as ours.

More specifically, the preceding comparison reveals that we are not interested in the degree of localization $\sum_{\ell \in \mathrm{Box}_k(\epsilon)} |\psi_\ell|^2$ of the *equilibrium* eigenstates of the system. Rather we are interested in how an excitation $|k\rangle$ localized at a single node k, which corresponds to a *highly non-equilibrium state*, propagates through the system, and its probability of 'touching' another node ℓ later. In the case of Anderson localization, a local excitation would not propagate much, so at best there would be a very small probability of transfer to nearby nodes and none for transfer to distant nodes, and the ITF graph would be the disconnected union of many small order subgraphs *of low ITF edges.*

3.6. Comparison with strong multifractality MBL [26]

There is one case where the traditional localization yields results close to our concept of localization. The strong multifractality MBL of [26, Eq. (18)] relies on the partition function $\sum_\ell |\langle \psi_k | \sigma_Z^N | \psi_\ell \rangle|^{2q}$ and yields a spectrum $f(\alpha)$ close to what has been observed in some cases. Looking at Figs. 6(d) and (f), it appears that rings of size $N = 105$ and $N = 500$ show a Multi-Body-Localization transition as the bias approaches 50. On the other hand, Fig. 5(f) reveals that Multi-Body-Localization only occurs for some ring size.

4. Multi-fractal analysis of chains

One important spin network topology is represented by spin chains (see top left hand side of Fig. 2). To investigate the geometrical properties of a chain of spins, we use the information-metric-based mapping (see Fig. 2) and estimate the partition function as a function of the order q of higher order moments as described in Eq. (12). The observed statistical self-similarity (see Fig. 1) of the spin network translates into a power law relationship of the partition function and allows us to estimate the generalized Hurst exponent $H(q)$ and the multi-fractal spectrum $f(\alpha)$.

Fig. 3(a) shows the generalized Hurst exponent as a function of order q for several spin chain lengths (i.e., $N =$ 100, 102, 106, 108, 112, 126, 130, 136, 138, 148, and 150). The generalized Hurst exponent $H(q)$ displays a sigmoidal shape irrespective of the spin chain length. Similar sigmoidal shapes are observed for numerous other spin chain lengths. Fig. 3(d) summarizes the $H(q)$ vs q dependency for spin chain lengths of $N = 700, 708, 718, 726, 732, 738, 742, 750, 756, 760, 768, 772, 786$ and 796. This sigmoidal pattern shows that the information metric graph, having a heterogeneous architecture, is better characterized by multi-fractal geometric tools. Generally speaking, this implies that a single fractal dimension is insufficient to model the (heterogeneous) interactions and information transmission / propagation in the spin chain.

All of chain lengths N considered above are such that all eigenvectors of the (single excitation subspace) Hamiltonian are completely delocalized, i.e., *all* eigenvectors have non-zero overlap with *all* nodes.

In addition to the sigmoidal shape, we also observe that for some lengths of the spin chain the generalized Hurst exponent exhibits a much more complex nonlinear dependency as a function of the qth order moment (see Fig. 5(a) summarizing the analysis for spin chain lengths of $N = 105, 115, 119, 129,$ and 149).

We also note that these particular spin chain lengths exhibit higher generalized Hurst exponents than those in Figs. 3(a) and (d). This suggests that some spin chains exhibit a pronounced persistent behavior, i.e., a long interaction is likely to favor an even longer one, while others tend to display an anti-persistent behavior, interleaving short with long interactions. From a practical perspective, it would be interesting to investigate the information processing / transmission properties of these two classes of spin chains on real devices, which may show some to be more suitable for information transmission while others might be better suited for robust information storage or parallel processing.

An alternative strategy for describing the local self-similar (scaling) properties of the information graph and quantify the degree of heterogeneity is to estimate the multi-fractal spectrum. From a mathematical perspective, the multi-fractal spectrum represents the set of Lipschitz–Hölder exponents (fractal dimensions) and their likelihood of appearance as dictated by the mixture of locally self-similar motifs in the informational graph. Consequently, by estimating and analyzing the multi-fractal spectrum we can learn the existing dominance of some Lipschitz–Hölder exponents over others. The Lipschitz–Hölder exponent quantifies the local singularities and locates the abrupt changes in the curvature of information graph embedding. More precisely, the maximum of the multi-fractal spectrum represents the dominant fractal dimension while the width of the spectrum is a measure of the heterogeneity richness (range of fractal dimensions) and complexity. From a structural point of view, the multi-fractality implies that the information graph consists of regions of short interactions (short information transmission ranges) mixed / interspersed with long-range interactions. Figs. 3(b) and (e) show the multi-fractal spectrum for several spin chain lengths. We observe that even though the generalized Hurst exponent for all these chain lengths exhibits a similar sigmoidal shape, the multi-fractal spectrum displays different and asymmetric behavior. For instance, the multi-fractal spectrum of the spin chain of length $N = 102$ is prolonged over higher Lipschitz–Hölder exponents and thus stronger singularities, while the multi-fractal spectrum of the chain of size $N = 130$ is extending more towards lower Lipschitz–Hölder exponents corresponding to lower singularities in the curvature of the informational embedding.

The existence of these singularities in the information embedding suggests building on the multi-fractal analysis to develop a thermodynamic formalism of information propagation through the spin networks. Of note, this thermodynamic formalism is not aimed at quantifying fluctuations over time but rather the spatially self-similar behavior in information transfer through a spin network. To elucidate the existence of a phase transition, we investigated the behavior of a thermodynamics inspired specific heat derived from the estimated partition function. Figs. 3(c) and (f) show that the specific heat exhibits a bell shape whose peak values occur for various orders of q. In contrast, the specific heat for spin chains of lengths $N = 105, 115, 119, 129,$ and 149 in Fig. 5(b) display a much more complex behavior that seems to be discontinuous in the vicinity of order $q = 0$.

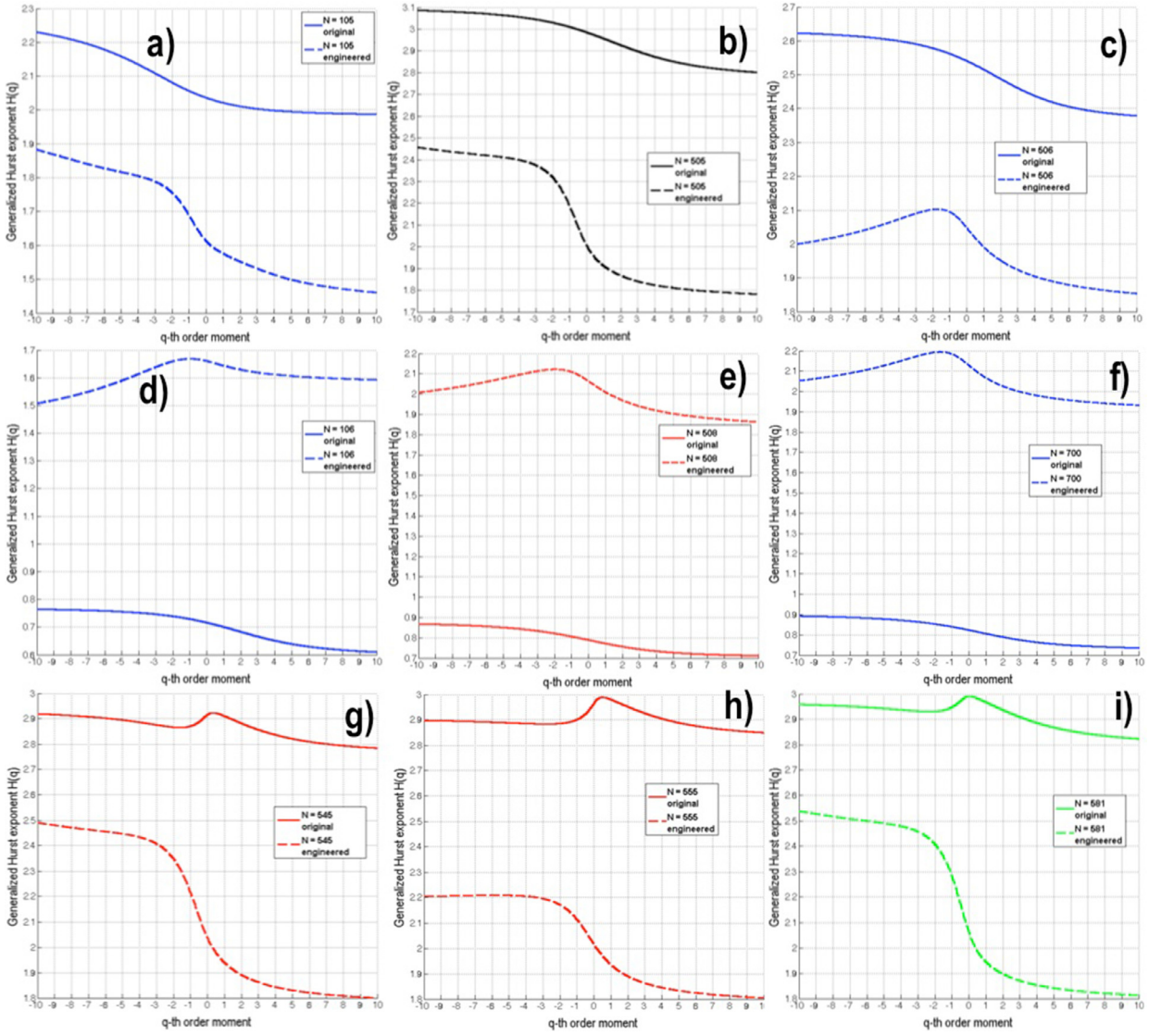

Fig. 4. Comparison between original and engineered spin chains in terms of generalized Hurst exponent $H(q)$ for various chain lengths: (a) $N = 105$, (b) $N = 505$, (c) $N = 506$, (d) $N = 106$, (e) $N = 508$, (f) $N = 700$, (g) $N = 545$, (h) $N = 555$, and (i) $N = 581$.

5. Multi-fractal analysis of rings

While spin chains have been most intensively studied in recent years, other arrangements such as rings also play an important role for quantum spintronic applications as their translation invariance properties make them potentially suitable as routers for quantum networks. Consequently, it is important to study their information propagation characteristics. We have estimated the ITF metric for several ring sizes (i.e., from $N = 50, \ldots, 1000$), mapped the information propagation between all distinct pair of nodes $|i\rangle$ and $|j\rangle$, and applied our strategy for estimating the partition function over the metric graph. Figs. 5(c) and (e) summarize the generalized Hurst exponents as a function of the qth order moment for several spin ring lengths. One observation we could make is that while the generalized Hurst exponents in Fig. 5(c) are higher and reminiscent of a persistent dynamics, the generalized Hurst exponents in Fig. 5(e) are much smaller (a third of those in Fig. 5(c) and closer to 0.5) which would indicate a tendency of an anti-persistent structure. This distinction is even more interesting as it appears between spin rings of similar sizes. We have analyzed all spin rings $N =$ 50–1000 and we observed similar patterns. Consequently, it would be important to quantify the design implications and transmission properties against realistic devices.

Another observation we could make from Figs. 5(c) and (e) is that most of the spin rings display a similar sigmoidal shape observed also for some spin chains, but a few spin rings (e.g., for $N = 106$ and 130) exhibit a generalized Hurst exponent that varies very little with order q. This can also be seen from the multi-fractal spectrum plots in Figs. 5(d) and (f). For spin rings of sizes $N = 106$ and 130, we could conclude that are more closer to displaying a mono-fractal behavior (due to their lower generalized Hurst exponents and shrinking of their multi-fractal spectrum).

Spin rings are of interest as they can act as quantum routers in internet-on-a-chip architectures. Rings can be “quenched” by applying a very strong bias (magnetic field) on one spin; this has the effect of favoring transmissions symmetric relative to the bias and at the limit of infinite bias the ring is “quenched” to a chain with perfect information transfer fidelity between nodes next to the quench node. Consequently, we studied the multi-fractal characteristics of spin rings as a function of the magnitude of applied bias. For instance, Figs. 6(a) and (b) summarize the generalized Hurst exponent and the multi-fractal spectrum obtained for

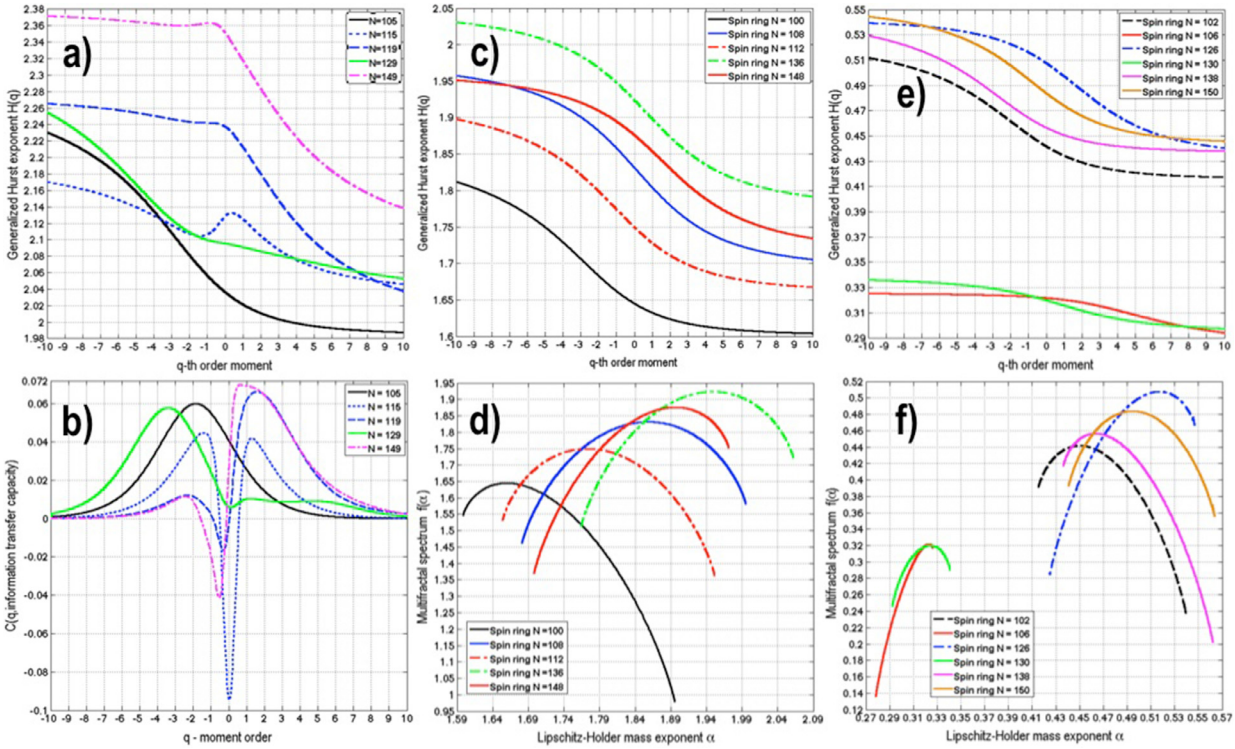

Fig. 5. (a) Generalized Hurst exponent $H(q)$ as a function of q for spin chain lengths of $N = 105, 115, 119, 129,$ and 149 display a highly nonlinear behavior corresponding to rich multi-fractality. (b) Specific heat $C(q)$ for spin chain lengths of $N = 105, 115, 119, 129,$ and 149 exhibits a rich behavior that could be correlated to either a first- or a second-order (informational) phase transition. (c) Generalized Hurst exponent $H(q)$ as a function of q for several spin ring lengths (i.e., $N = 100, 108, 112, 136,$ and 148) displaying a similar "sigmoidal" shape. (e) The generalized Hurst exponent $H(q)$ as a function of q for spin ring lengths of $N = 102, 126, 130, 138,$ and 140 display a more pronounced multi-fractal behavior than for sizes of $N = 106$ and 130. (f) Comparison in terms of multi-fractal spectrum (shape and width) between spin ring networks of size $N = 102, 106, 126, 130, 138,$ 140 and 150. Note that the red multifractal spectrum curve, bias = 106, passes through the point $f(2.75) = 1.4$, a manifestation of the strong multifractal property $f(0 \le \alpha \le 2) = \alpha/2$ of [26]. (For interpretation of the references to colour in this figure legend, the reader is referred to the web version of this article.)

an information-metric embedding of a spin ring of size $N = 102$ when the bias is applied to node 100 (the magnitude of the bias is assumed to take integer values between 0 and 10). We observe from Fig. 6(a) that with increasing bias the generalized Hurst exponent is shifting towards higher values. We also notice that the increase in the width of the generalized Hurst exponent is not monotonic with increasing bias magnitudes. This multi-fractal trend (of higher multi-fractality for non-zero bias) is also confirmed by the multi-fractal spectrum plot in Fig. 6(b). To further investigate this behavior, Figs. 6(c) and (d) summarize the generalized Hurst exponent and the multi-fractal spectrum of the same configuration (spin ring of size $N = 102$) for bias magnitudes of 0, 5, 10, 20, 50 and 100. We notice that with increasing bias magnitudes the support of the multi-fractal spectrum shifts towards left, an anti-persistent region. To contrast these results, Figs. 6(e) and (f) show the generalized Hurst exponent and the multi-fractal spectrum for a spin ring of size $N = 500$ and the bias is applied at node 100. We observe that while the generalized Hurst exponent is significantly wider for nonzero bias, the multi-fractal spectrum in Fig. 6(f) displays a similar tendency of shifting towards left. We suspect that the multi-fractality of both original and "quenched" spin rings is not only affected by the number-theoretic properties of the ring but also by the bias magnitudes. We plan to investigate these suppositions both analytically and experimentally in the future.

6. From thermalization to localization

Following the early definition of Section 2.1, thermalization [27–29] in its limiting case could be interpreted as $p_{\max}$ uniformly distributed for $i \neq j$. This implies that the α_k's are the same across all sites; hence the spectrum is monofractal.

Localization on the other hand in its early and extreme definition means $p_{\max}(i, j) = \delta_{i,j}$. Hence $d(i, j) = 0$ if $i = j$ and $d(i, j) = \infty$ if $i \neq j$. In this situation, $\forall \epsilon$ *finite*, the ϵ-covering of the whole graph requires a ball around every single site, so that $n_\alpha = w(\alpha)\epsilon^{-f(\alpha)} = N$. At this stage, it is essential to recall the relationship $N\epsilon = 1$, in which case $w(\alpha)\epsilon^{-f(\alpha)+1} = 1$. The independence of the latter on ϵ implies that $f(\alpha) = 1$, that is, a flat spectrum. We observe a flattening in the multi-fractal spectrum in Figs. 6(b), (d) and (f) with increasing magnitude of the bias. However, the flattening is not complete and we suspect that the cause of this is related to the finite size effects of the considered rings.

To exemplify some of the "inbetween" cases, we should imagine that the system transitions from uniformity to a more skewed distribution measure μ. This implies that, while initially the measure μ satisfies $\mu = c_k\epsilon^{\alpha_k} = 1$, it will slightly lose mass and redistribute this mass due to phase transition towards the tail becoming $\mu = c_k\epsilon^{\alpha_k} = \epsilon^{\xi_1}$. By the same token of a phase transition, the average number $n_\alpha = w(\alpha)\epsilon^{-f(\alpha)} = 1/\epsilon$ will transition to a power law scaling of the form $n_\alpha = w(\alpha)\epsilon^{-f(\alpha)} = \epsilon^{-\xi_2}$. By corroborating these two facts we obtain that $f(\alpha) = \alpha\xi_2/\xi_1$. The latter is a generalization of the theoretical strong multi-fractality spectrum condition $f(0 \le \alpha \le 2) = \alpha/2$, singled out in [26]. This heuristic derivation and resemblance with the multi-fractality spectrum condition mentioned in [26] indicates that the slope and shape of the multi-fractal spectrum for quantum spin networks depends in a nontrivial way not only on the applied bias or couplings, but also on their size and topology. We plan to investigate these intuitions analytically and in simulation in our future work.

Note that $\mu = c_k\epsilon^{\alpha_k} = 1$ means thermalization at a low scale, while moving the mass towards the tail means localization at a larger scale. Therefore, the preceding is a case of *phase transi-*

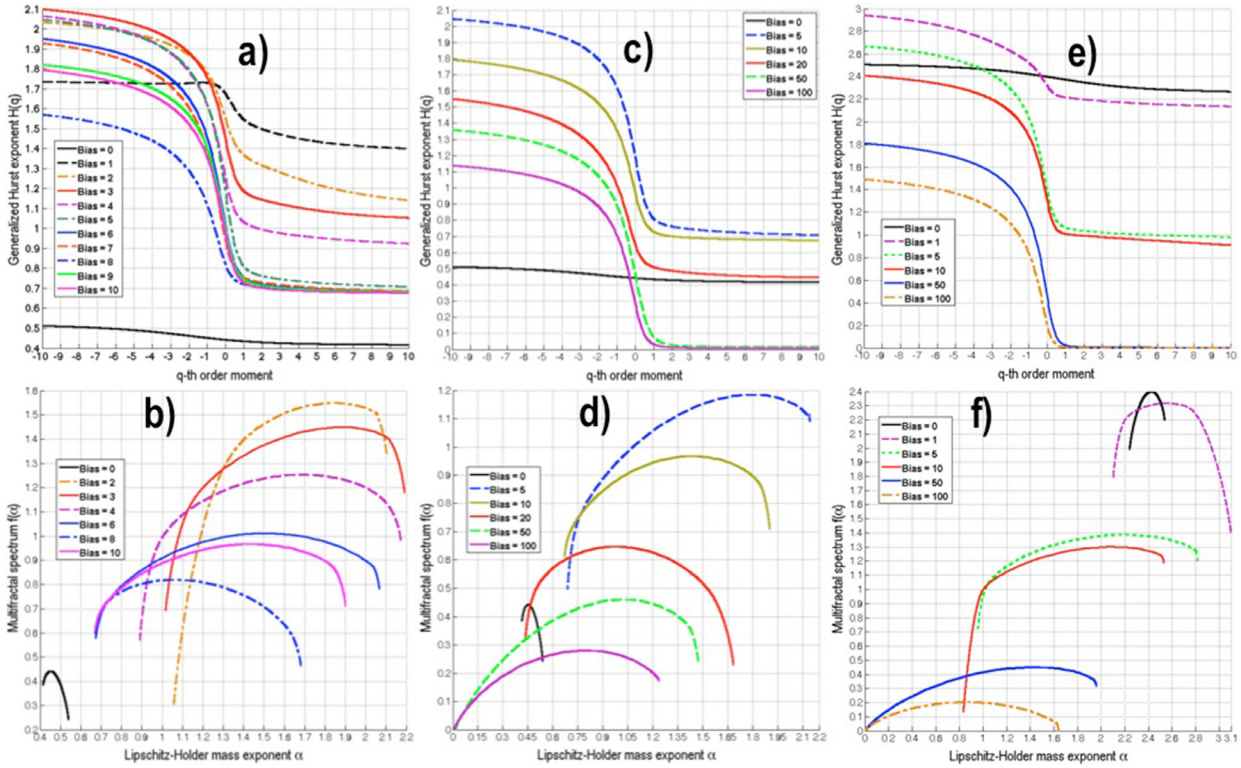

Fig. 6. (a) Generalized Hurst exponent (GHE) $H(q)$ as a function of q for spin ring of length $N = 102$ and a bias B of 0, 1, 2, 3, 4, 5, 6, 7, 8, 9, and 10 applied to node 100. The GHE displays a highly nonlinear behavior for non-zero bias B which corresponds to a richer multi-fractality. (b) The multi-fractal spectrum for a ring of length $N = 102$ and a bias B of 0, 2, 3, 4, 6, 8 and 10. (c) The GHE $H(q)$ as a function of q spin ring of length $N = 102$ and a bias B of 0, 5, 10, 20, 50, and 100. (d) The multi-fractal spectrum for the ring of size $N = 102$ and a bias B of 0, 5, 10, 20, 50 and 100. Observe that for biases 50, 100, the slope of the multifractality spectrum in roughly 1/2, in agreement with the condition $f(0 \le \alpha \le 2) = \alpha/2$ of [26]. (e) The GHE $H(q)$ as a function of q for a spin ring of length $N = 500$ and a bias B of 0, 1, 5, 10, 50, and 100. (f) The multi-fractal spectrum for a spin ring of length $N = 500$ and a bias B of 0, 1, 5, 10, 50, and 100. This last case-study clearly shows sign of a MBL transition as the bias gets close to 50 (blue curve); it is indeed noted that the blue fractal spectrum curve of bias 50, and to a more accurate extent the yellow curve of bias 100, have their slope roughly equal to 1/2 around $\alpha = 0$, in agreement with the theoretical strong multifractality spectrum condition $f(0 \le \alpha \le 2) = \alpha/2$, singled out in [26]. Note that for biases from 0 to 10 none of that behavior is observed. (For interpretation of the references to colour in this figure legend, the reader is referred to the web version of this article.)

tion to localization, concomitant to the multi-fractal spectrum going from δ-distributed to linear in α. To some extent, this can be visually observed for ring topologies with various bias magnitudes in Figs. 6(b), (d) and (f).

7. Discussion

It is our belief that the complex ITF behavior exhibited by spin networks is a matter of their scaling properties. By analyzing spin chains and rings up to size 1000 we observe that they display complex mono-fractal/multi-fractal structure depending on their symmetry. In addition, a thermodynamics inspired framework reveals that several such spin chains and rings exhibit some forms of phase transition which could prove fundamental in the design of these future devices.

The spin chain results suggest that information transmission in spin networks not only exhibits complex multi-fractal behavior but also nontrivial dependence on the size of the network. Previous work on ITF bounds and their attainability [11,15] has shown that the size of the network, N, and various number theoretic issues play a role. Our multi-fractal analysis appears to corroborate the observations made in prior studies and open the possibility to establish a connection between these fields. In addition to N, it was shown in [11] that the ITF depends on the greatest common divisor $\gcd(i, j)$, where i and j are the input and output spins, respectively. The somewhat repetitive pattern of $\gcd(i, j)$ may be the root cause underpinning the multi-fractality.

In a near technological future, chains will probably have their coupling strength engineered to favor specific transfers. It would be interesting to compare the multi-fractal properties such as the width and shape of the generalized Hurst exponent of engineered chains with those of a chain with uniform coupling. Fig. 4 shows some interesting trends from which we draw the following observations:

- The engineered chains have higher multi-fractality as evidenced by the increasing width of the generalized Hurst exponent.
- The spin chains exhibit a dichotomous behavior in the sense that as a result of applying an engineered strategy in some cases it makes the generalized Hurst exponent shift above the original one while in other cases it shifts below the original one.

As far as rings are concerned, for zero bias, they show a very narrow multi-fractal spectrum, revealing that the symmetry contributes to mono-fractality. However, rings can be endowed with a non-trivial potential landscape that changes the onsite potentials, corresponding to the diagonal elements in the Hamiltonian. As the bias increases we observe a higher degree of multi-fractality, consistent with the shape of the multi-fractal spectrum of the engineered spin chains.

The ITF developed here is an upper bound that becomes relevant when enough time is given for the i to j transfer to achieve its maximum fidelity. As already emphasized in [11,15], $|\langle j|\exp(-\imath Ht/\hbar)|i\rangle|$ exhibits a complex, somewhat repetitive time dependence. This indicates that a spatio-temporal fractal analysis is warranted, but this is left for further research.

For both spin chains and rings, we find that the degree of multi-fractality varies with network sizes. Engineered spin chains

display a more pronounced multi-fractal behavior than the original counterparts. Along the same lines, we observe that the degree of multi-fractality for spin rings is influenced by the considered bias magnitude.

Finally, we must recognize that there seems to be some relationship between the many-body-localization (MBL) [27–29] and the quantum phase transition we observe in the information transfer capacity. As discussed in [27–29], a quantum phase transition is observed as one varies the disorder strength or the energy density between the thermal phase and the MBL phase. In the MBL, all the eigenstates do not obey the eigenstate thermalization hypothesis (ETH) and the memory of local initial conditions can survive in local observables for arbitrary long times. This seems to be the case in our analysis which encodes the interaction strength, temperature, size and topology of the spin network into a information theoretic metric (namely the information transfer fidelity) and weighted graph mapping. We believe that the mathematical formalism presented in this paper with some significant extensions can help at overcoming the finite-size scaling issues and elucidating the nature of quantum phase transition, gauging the impact of control parameters such as the interaction and disorder strength and temperature. This multi-fractal formalism could also suggest new avenues for studying the vicinity of the critical points.

Acknowledgments

P.B. acknowledges support from US National Science Foundation (NSF) under CAREER Award CPS-1453860 and CyberSEES CCF-1331610 grants, and the US Army Defense Advanced Research Projects Agency (DARPA) under grant number W911NF-17-1-0076 and DARPA Young Faculty Award under grant number N66001-17-1-4044. E.J. was partially supported by the Army Research Office (ARO) Multi University Research Initiative (MURI) grant W911NF-11-1-0268. S.S. acknowledges support from the Ser Cymru National Research Network on Advanced Engineering and funding from a Royal Society Leverhulme Trust Senior Fellowship.

References

[1] Aldrovandi R, Pereira JG. An introduction to geometrical physics. World Scientific; 1999.
[2] Awschalom DD, Bassett LC, Dzurak AS, Hu EL, Petta JR. Quantum spintronics: engineering and manipulating atom-like spins in semiconductors. Science 2013;339(6124):1174–9.
[3] Bagguley DMS, Griffith JHE. Paramagnetic resonance and magnetic energy levels in chrome alum. Nature 1947;160:532–3.
[4] Kantelhardt JW, Zschiegner SA, Koscielny-Bunde E, Havlin S, Bunde A, Stanley HE. Multifractal detrended fluctuation analysis of nonstationary time series. Physica A 2002;316(1):87–114.
[5] Bose S. Quantum communication through spin chain dynamics: an introductory overview. Contemp Phys 2007;48(1):13–30.
[6] Breuer HP, Petruccione F. The theory of open quantum systems. Oxford University Press; 2002.
[7] Chhabra A, Jensen RV. Direct determination of the f(α) singularity spectrum. Phys Rev Lett 1989;62:1327–30.
[8] Christandl M, Datta N, Dorlas TC, Ekert A, Kay A, Landahl AJ. Perfect transfer of arbitrary states in quantum spin networks. Phys Rev A 2005;71:032312.
[9] Christandl M, Datta N, Ekert A, Landahl AJ. Perfect state transfer in quantum spin networks. Phys Rev Lett 2004;92:187902.
[10] Ernst RR, Bodenhausen G, Wokaun A. Principles of nuclear magnetic resonance in one and two dimensions. International series of monographs on chemistry. Clarendon Press; 1990.
[11] Jonckheere E, Langbein FC, Schirmer S. Quantum networks: anti-core of spin chains. Quantum Inf Process 2014;13(7):1607–37.
[12] Jonckheere E, Langbein FC, Schirmer SG. Curvature of quantum rings. In: Communications control and signal processing (ISCCSP), 2012 5th international symposium on; 2012. p. 1–6.
[13] Jonckheere E, Schirmer SG, Langbein FC. Geometry and curvature of spin networks. In: Control applications (CCA), 2011 IEEE international conference on. IEEE; 2011. p. 786–91.
[14] Lee J, Stanley HE. Phase transition in the multifractal spectrum of diffusion-limited aggregation. Phys Rev Lett 1988;61.
[15] Jonckheere E, Langbein F, Schirmer S. Information transfer fidelity in spin networks and ring-based quantum routers. Quantum Inf Process 2015;14(12):4751–85. arXiv:1408.3765. (arXiv preprint 2014).
[16] Kay A. Perfect, efficient, state transfer and its application as a constructive tool. Int J Quant Inf 2010;08(04):641–76.
[17] Khajetoorians AA, Wiebe J, Chilian B, Wiesendanger R. Realizing all-spinbased logic operations atom by atom. Science 2011;332(6033):1062–4.
[18] Langbein F, Schirmer S, Jonckheere E. Time optimal information transfer in spintronics networks. In: 2015 IEEE conference on decision and control (CDC); 2015. p. 6454–9. ArXiv preprint arXiv:1508.00928
[19] Lauterbur PC. C13 nuclear magnetic resonance spectra. J Chem Phys 1957;26(1):217–18.
[20] Lund A, Shimada S, Shiotani M. Principles and applications of ESR spectroscopy. Principles and applications of ESR spectroscopy. Springer; 2011.
[21] Mandelbrot BB. The fractal geometry of nature. W. H. Freedman and Co., New York; 1983.
[22] McRobbie DW, Moore EA, Graves MJ, Prince MR. MRI from picture to proton. Cambridge University Press; 2006.
[23] Meisel LV, Johnson M, Cote PJ. Box-counting multifractal analysis. Phys Rev A 1992;45:6989–96.
[24] Rodriguez A, Vasquez LJ, Slevin K, Römer R. Multifractal finite-size-scaling and universality at Anderson transition 2011;28. arXiv:1107.5736v1. [cond-mat.dis-m], July.
[25] Wolf SA, Awschalom DD, Buhrman RA, Daughton JM, von Molnar S, Roukes ML, et al. Spintronics: a spin-based electronics vision for the future – wolf et al. 294 (5546): 1488 – science. Science 2001;294:1488–95. doi:10.1126/science.1065389.
[26] Monthus C. Many-body-localization transition: strong multifractality spectrum for matrix elements of local operators 2016;12. arXiv:1603.04701v2. [cond-matt-nn].
[27] Nandkishore R, Huse DA. Many-body localization and thermalization in quantum statistical mechanics. Annu Rev Condens Matter Phys 2015;6:5–38. (Volume publication date March 2015).
[28] Altman E, Vosk R. Universal dynamics and renormalization in many-body-localized systems. Annu Rev Condens Matter Phys 2015;6:383–409. (Volume publication date March 2015).
[29] Vasseur R, Moore JE. Nonequilibrium quantum dynamics and transport: from integrability to many-body localization. J Stat Mech 2016;2016.